LBL-38343
UC-419

ERNEST ORLANDO LAWRENCE
BERKELEY NATIONAL LABORATORY

Diagnostics for Induction Accelerators

T.J. Fessenden
Accelerator and Fusion
Research Division

April 1996

LBL-38523
UC-419
HIFAN 811

Diagnostics for Induction Accelerators

Thomas J. Fessenden
Accelerator & Fusion Research Division
Lawrence Berkeley National Laboratory
University of California
Berkeley, California 94720

*This work was supported by the Director, Office of Energy Research, Office of Fusion Energy, U.S. Dept. of Energy, under Contract No. DE-AC03-76SF00098.

LBL 38523

HIFAN 811

Diagnostics for Induction Accelerators

Thomas J. Fessenden

Lawrence Berkeley National Laboratory

Berkeley, CA 94720

Abstract

The induction accelerator was conceived by N. C. Christofilos and first realized as the Astron accelerator that operated at LLNL from the early 1960's to the end of 1975. This accelerator generated electron beams at energies near 6 MeV with typical currents of 600 Amperes in 400 ns pulses. The Advanced Test Accelerator (ATA) built at Livermore's Site 300 produced 10,000 Ampere beams with pulse widths of 70 ns at energies approaching 50 MeV. Several other electron and ion induction accelerators have been fabricated at LLNL and LBNL. This paper reviews the principal diagnostics developed through efforts by scientists at both laboratories for measuring the current, position, energy, and emittance of beams generated by these high current, short pulse accelerators. Many of these diagnostics are closely related to those developed for other accelerators. However, the very fast and intense current pulses often require special diagnostic techniques and considerations. The physics and design of the more unique diagnostics developed for electron induction accelerators are presented and discussed in detail.

INTRODUCTION

Induction accelerators are low impedance devices and able to accelerate beams at currents much greater that from rf based accelerators. Electron current pulses are typically measured in kiloamps with pulse times measured in nanoseconds and contains no micro structure. The accelerating voltage is isolated from the outside world by inductors that must support the total accelerating voltage for the duration of each pulse. Diagnostics for induction accelerators must reproduce the waveforms of the accelerator parameters with great fidelity. Fortunately, the large currents and voltages typical of an induction accelerator are easily detected and small signal levels are not usually a concern.

This paper focuses on the very fast beam monitors developed for measuring the current and position of high-current electron beams in induction accelerators. Also described are two systems for measuring the beam energy in the Astron and ATA accelerators; X-ray wire scanning techniques for determining beam profiles; and two methods of measuring pulsed magnetic fields in a harsh environment. Most of this work dates back to 70s and early 80s when electron induction linacs and their diagnostics were under intensive development. Many of these diagnostics are also summarized in a paper presented by K. W. Struve (1) at a conference at the Bureau of Standards in Gaithersburg, Maryland in 1986.

INDUCTION ACCELERATORS

The linear induction accelerator was invented by N. C. Christofilos in about 1960 for the purpose of generating the "E-layer" for the Astron thermonuclear fusion experiment. Even in the proof-of-principle experiment then under development at the Lawrence Livermore Laboratory, the Astron concept (2) required relativistic electrons at currents far beyond those available from conventional accelerators. The Astron accelerator (3) was developed as a part of this program and, near the end of its operational life, produced 400 ns pulses of 6 MeV electrons at currents up to 800 Amperes. The accelerator could be operated at many repetition rates including a burst mode of 100 pulses at rep-rates up to 1440 Hz intended to build and maintain the E-layer. The accelerator normally operated at an average repetition rate of 2 Hz set mainly by considerations of x-radiation levels at neighboring laboratory experiments. The accelerator used cable pulse forming lines switched by hydrogen thyratrons to generate square current pulses with a rise time near 10 ns. The Astron accelerator was in operation from 1961 through 1975. The Astron accelerator technology was further advanced by a development (4) under J. Leiss at the National Bureau of Standards during the mid 70s aimed at extending the pulse width and reducing the cost of the expensive induction cores that are a part of this accelerator concept. This machine was transferred to the Naval Research Laboratory in the early 80s for use as the driver for a free electron laser experiment.

The Astron accelerator was followed by the ERA accelerator (5) at Lawrence Berkeley Laboratory in 1972. This machine used oil Blumlein pulse forming lines switched by spark gaps to generate 30 ns pulses of electrons at currents up to 3 kA and energies near 4 MeV. The accelerator was used for research on the electron ring collective accelerator concept at the Lawrence Berkeley Laboratory. This accelerator was followed by three related accelerators at the Lawrence Livermore Laboratory: the ETA accelerator (6) in 1979 *(10 kA, 4.5 MeV, 40 ns, 1 Hz)*; the FXR accelerator (7) in 1982 *(4 kA, 20 MeV, 60 ns, 1/3 Hz)*; and the ATA accelerator (8) in 1984 *(10 kA, 50 MeV, 70 ns, 1 Hz average or 10 pulse burst at 1 kHz)*. These three accelerators used water filled Blumlein pulse-forming-lines and spark gap switches. The ETA and ATA accelerators were part of the Strategic Defense Initiative and the FXR accelerator is used for flash radiography. An ETA II (9) accelerator that used magnetic modulator technology operated briefly in the late 1980s.

A four-beam ion induction linac named MBE-4 (10) was built and operated from 1986 to 1991. This machine accelerated four parallel beams of cesium$^+$ to nearly 1 MeV while increasing the current from 4 x 10 mA to nearly 4 x 90 mA. This proof-of-principal experiment was part of the Heavy Ion Fusion Accelerator Research program at the Lawrence Berkeley Laboratory. A recirculating ion induction accelerator (11) is currently being fabricated at LLNL to demonstrate the physics of this approach to a more economical heavy ion fusion accelerator/driver. Diagnostics developed for this accelerator were discussed by S. Eylon (12) and D. Berners with L. Reginato (13) at previous Beam Instrumentation conferences.

Of all these induction accelerators, only the FXR machine is currently in operation.

CURRENT AND POSITION MEASUREMENTS--BEAM BUGS

Introduction

Perhaps the most important diagnostics developed for induction accelerators is the device that monitors the beam current and position in the accelerator and associated beam transport lines. These instruments commonly called "beam bugs" are capable of measuring the kiloampere currents and beam position of the ETA and ATA accelerators with rise times of less than 0.2 ns and relative position resolutions less than 100 μm. They operate by measuring the currents induced in the wall by the passage of the beam.

One of the first to use this technique for monitoring beam current and position was a team (14) at the Lawrence Berkeley Laboratory. They used a band of resistors to interrupt the wall current and generate a current and position signal from the beam in the ERA accelerator. The idea was rapidly adapted for use on the Astron accelerator (15) at Livermore. Fifty one-ohm carbon resistors were placed in the tube wall at nearly 30 locations along the Astron accelerator and transport section.

For the ETA and ATA accelerators, the carbon resistors were replaced by a one mil thick (27 μm) foil or band of stainless steel that is laser or E-beam welded across an insulated break in the beam tube wall. The diameter of the band equals the inner diameter of the beam tube so that the beam sees no abrupt steps or extraneous capacitance during its passage through the bug. A small overlap is formed as the band encircles the inside diameter of the tube. As we will show later, this overlap limits the absolute accuracy of the beam position measurements to a few tenths of a millimeter. Fig. 1 shows the design (16) of the beam "bug" used with the ATA accelerator. The resistance of the resistor foil was approximately two milli-Ohms with a resulting sensitivity of the instrument of 1 kA/V. Also shown are measurements of the response of the bug to a 10 amp fast rising current pulse from a test pulser. A ferrite inductor is placed behind the resistor foil to prevent the beam current from flowing around the resistor. Because of the very low foil resistance, the L/R time for the current to decay is very much longer than the beam pulse. A polyimide ring is used to form an insulating vacuum seal. To achieve the very high frequency response of this instrument we found it necessary to reduce the capacitance of the insulating gap by using a thick polyimide ring. Eight pickoffs as shown in Fig. 1 are used to develop the current and position signals. These are brought out through 50 Ω resistors as shown to keep the cables matched.

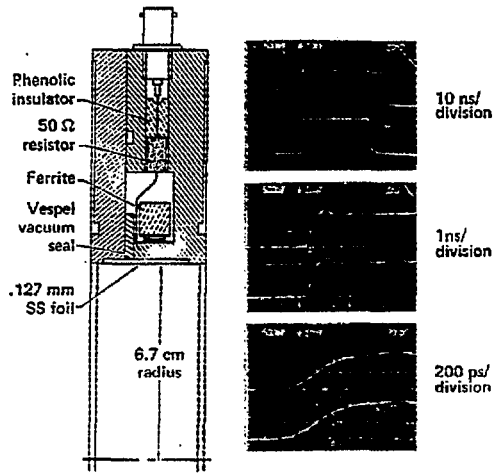

Fig. 1 Drawing of an ATA beam bug. Also shown is the response of the bug (lower trace) to a 10 Amp pulse (upper trace) along the bug axis from a mercury pulser.

THEORY

R.C. Weber (17) has described some of the physics of this type of monitor in the first of these beam instrumentation meetings. He describes the wall currents flowing near a beam bug or wall current monitor but considers the performance of a monitor with a much larger resistance than of interest here. Let us extend his arguments with a more quantitative analysis of the physics of a beam in a conducting pipe.

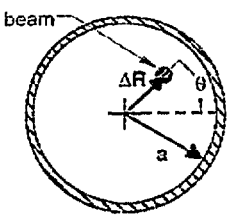

Fig. 2 Sketch of a beam off axis in a conducting pipe

It is possible to show (by the method of images for example) that a current I flowing within a pipe of radius a at a distance ΔR off axis causes a surface current $K(\theta)$ to flow on the inner pipe wall that is given by

$$K(\theta) = (I/2\pi a)\left[(\rho^2-1)/(1+\rho^2-2\rho\cos\theta)\right] . \qquad (1)$$

where $\rho = \Delta R/a$. The angle θ is defined by Fig. 2. Consider interrupting the beam pipe with a resistive band or ring placed at the inner circumference of the pipe with total resistance R. The surface current $K(\theta)$ passing through the resistor that initially or for a short time develops a voltage around the pipe $V(\theta)$ given by

$$V(\theta) = K(\theta)\,2\pi a\,R = RI\,\frac{\rho^2-1}{1+\rho^2-2\rho\cos\theta} . \qquad (2)$$

However, the voltage variation around the pipe will drive a current that flows through the gap to the outside of the pipe, that will equalize this voltage. After equalization, the surface current pattern on the outside of the pipe may look something like that sketched in Fig. 3 and the voltage across the gap will be independent of θ and given by $V(\theta) = I\,R$. However, until the current leaks through the gap, both beam current and position measurements are possible.

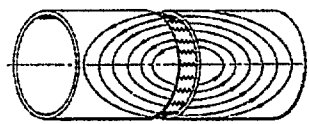

Fig. 3 Sketch of the current pattern eventually established on the outside of the pipe as a result of the resistive band

As we will show, the leakage field pattern is approached approximately exponentially with a time constant that varies directly as the area of the pipe and inversely with resistor value R. For parameters used in the Astron accelerator (10-20 cm diameter, 20 mΩ shunt resistance), this time constant is a few tenths of a microsecond. Note that the lower shunt resistance of the ATA bug increases this time by a factor of about 10 but the ferrite does not slow down the establishment of this leakage current. We will return to the issue of this leakage current in a later section. Let us first assume that the beam pulse is short compared to the time for the leakage to occur. For this time the voltage around the gap is correctly given by Eq. (2).

The beam current signal is developed by adding the voltages from four pickoffs located 90° apart with a resistive summing circuit in which great care was taken to avoid reflections in the cabling. From Eq. 2 we find

$$V_I = 1/4 \quad [V(0) + V(90°) + (180°) + V(270°)]. \tag{3}$$

A little algebra yields

$$V_I = IR \frac{(\rho^4 - 1)(\rho^4 + 1)}{(\rho^4 + 1)^2 - 2\rho^4 (1 + \cos 4\theta)}. \tag{4}$$

Similarly, the position signals are obtained by adding a negative signal (pickoff goes the other way around the ferrite) at $180° + \theta$ to a positive signal at θ. Again we find

$$V_\rho = RI \frac{2\rho \cos\theta (1 - \rho^2)}{(1 + \rho^2)^2 - 2\rho^2 (1 + \cos 2\theta)}. \tag{5}$$

In the limit of small beam displacement from the axis ($\rho \ll 1$)

$$\boxed{V_I = RI} \tag{6}$$

and

$$V_\rho = 2\rho RI \cos\theta \tag{7}$$

or

$$\boxed{\frac{x}{a} = \rho_x = \frac{V_x}{2V_I}; \qquad \frac{y}{a} = \rho_y = \frac{V_y}{2V_I}} \tag{8}$$

These are the expressions used for finding the beam position within the transport system of the accelerator and beam transport line. The x or y position signal is digitized and divided by twice the current signal. Obviously, signal timing is extremely important and large errors can be expected at the beginning and end of the pulse.

Let us consider in detail the error in the current signal resulting from the assumption of small beam displacement ρ. Fig. 4 shows plots of the hypothetical current measured by the bug divided by the beam current as a function of the normalized beam displacement ρ. These curves were obtained from Eq. (5). The two curves show the bounds on the measurements to be expected for the case of the beam angle near a pickoff point and for the case of a beam half-way between two pickoff points. At a normalized displacement of $\rho = 1/2$, the error is less than or equal to $\pm$ 1/8. For displacements greater than $\rho = 1/2$ the error becomes very large. Therefore as a practical limit current measurements are of little value if the beam centroid is more than one-half the distance to the tube wall.

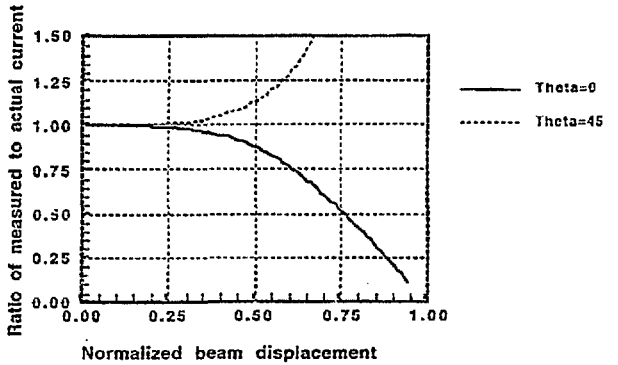

Fig. 4 Plot of the ratio of the measured to actual beam current as a function of the normalized beam displacement from axis. For arbitrary angle, the point will be bounded by the two curves.

A similar analysis of beam position measurements shows that position errors as large as $\pm$ 30% can be expected at normalized displacements ρ = 1/2.

Response at large time (Asymptotic Response)

Let us return to the issue of the leakage current and the way this current shorts out the position signal. This problem was considered by Cooper and Neil (18) and by Fessenden (19). Consider the sketch showing a transverse view of a beam bug as presented in Fig. 5. The beam axis and symmetry axis are vertical. The signal voltage V(θ) is isolated by the ferrite inductor from the foil of thickness δ and length ℓ_f. The ferrite is connected to the foil by two conducting rings separated by a gap ℓ_{gap}

Assume at t=0 that a beam induces a voltage across the foil given by Eq. (1) Because of the azimuthal voltage V(θ), a leakage current I(θ) will flow around the gap. This current flows on the area on either side of the gap at the foil and on the surfaces of the pipe. This current generates a magnetic field that flows in and out of the ferrite; through the foil; and into and out of the interior region of the pipe. Associated with this field is an inductance per unit length L. The determination of this inductance requires a solution of Maxwell's equations for the magnetic fields and surface current distributions in the region near the foils.

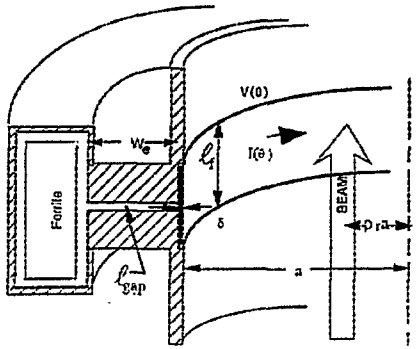

Fig.5 Cutaway sketch of an idealized beam bug.

As a very crude estimate let us assume that this azimuthal surface current only flows on both sides of the gap. With this approximation the inductance is found to be

$$L = \frac{\mu \ell_{gap}}{W_e} \quad . \tag{9}$$

In any case let us assume that Eq. (9) defines an effective width (W_e) such that L is the right value obtained from a proper solution to Maxwell's equations. For a gap $\ell_{gap} \ll a$, this value will be close to that shown in Fig. 1. We can now write a differential equation for V(θ) and I(θ), the voltage and current around the gap.

$$V(\theta_2) = V(\theta_1) - L\frac{dI(\theta)}{dt}\, a\Delta\theta \quad , \tag{10}$$

$$I(\theta_2) = I(\theta_1) - G\, a\Delta\theta \quad . \tag{11}$$

Here L is the inductance/m and G is the conductance/m around the, resistive foil and is given by

$$G = \frac{\sigma\delta}{\ell_f} \quad . \tag{12}$$

where σ is the conductivity of the foil material, δ is the foil thickness and ℓ_f is the length of the foil. Let us also define the fundamental time of the problem as

$$\tau = LGa^2 = \mu\sigma a^2 \frac{\delta}{W_e}\frac{\ell_{gap}}{\ell_f} \quad . \tag{13}$$

This time constant plays an important role in the work that follows. An estimate of its magnitude based on the dimensions given in Fig. 1 is near 1 μs.

We now have a differential equation for the voltage around the circumference of the gap given by

$$\frac{d^2V}{d\theta^2} = \tau\frac{dV}{dt} \quad . \tag{14}$$

The solution to this equation for the initial distribution given by Eq. (2) can be shown to be

$$V(\theta,t) = I_b R\left[1 + \sum_{n=1}^{\infty}\rho^n e^{-2n^2t/\tau}\cos n\theta\right] \quad , \tag{15}$$

Here I_b is the beam current. This equation has the required asymptotic time dependence since only the first term survives at large t. Substituting this into the x portion of Eq. (5) yields the expression for the displacement signal as a function of time.

$$V(x,t) = 2I_b R\left[\rho e^{-t/\tau}\cos\theta + \sum_{1}^{\infty}\rho^{2m+1} e^{-(2m+1)^2 t/\tau}\cos(2m+1)\theta\right] \quad . \tag{16}$$

Note that the first term decays with the time constant τ given by Eq. (13) and the higher order terms vanish rapidly. The y–position signal is described by a similar equation.

These relations show that, for times short compared to the time τ (≈ 1 μs), beam position measurements using beam bugs are possible with no further signal conditioning. The ETA and ATA accelerators had a pulse width of 40 to 70 ns. As a consequence, no conditioning of the position signal from the bugs used on these accelerators was necessary. For longer pulse accelerators such as the Astron accelerator, the decay of the position signal had to be extended. This was accomplished with a circuit of the type shown in Fig. 6

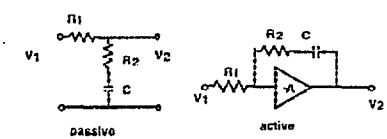

Fig 6 Simple compensation circuits for the beam bug position signals

The passive circuit has the transfer function

$$V_1 / V_2 = \frac{R_2}{R_1 + R_2} \frac{\left(s + 1/R_2C\right)}{\left(s + 1/\left(R_1 + R_2\right)C\right)} \qquad (17)$$

If R_2C is made equal to τ, the effective droop time is increased by the ratio $(R_1 + R_2)/R_2$ whereas the rise time is unchanged. The signal level is, of course, reduced by the same factor. In principle, perfect compensation can be obtained through the use of an operational amplifier as suggested in Fig. 6.

The beam current signal is generated by adding the voltage $V(\theta,t)$ at four equidistant points around the foil. Using Eq. (18) and proceeding as before gives

$$V_r(t) = 4I_bR\left[1 + \sum_{n=1}^{\infty} \rho^{4n}\, e^{-(4n)^2 t/\tau} \cos\left(4n\theta\right)\right] . \qquad (18)$$

Here the higher order terms vanish even faster than in Eq. (15) and no compensation is required.

Position errors resulting from the overlap

As mentioned before, beam bugs are fabricated using a strip of resistive material that is welded around the circumference with a small overlap. The overlap is necessary to prevent the large beam return current from generating noise signals within the bug. However, for the length of the overlap Δ, the azimuthal voltage $V(\theta)$ is one-half what it should be.

An analysis similar to the previous reveals that for a beam on axis the overlap will generate a voltage around the foil given by

$$V(r,t) = IR\left[1 - \frac{\Delta}{4\pi a} - \sum_{1}^{\infty} \frac{1}{2\pi n} \sin\frac{n\Delta}{2a}\, e^{-n^2 t/\tau} \cos\left(n\phi\right)\right] \qquad (19)$$

where ϕ is the angle to the overlap. Thus we see that the beam current measurement will be in error by a constant term plus a term that decays rapidly in time. This current measurement error is not as serious as the position error resulting from the foil overlap. For a small overlap Δ/a that is away from any pickoff, we find the major contribution to the x or position signal of

$$V_e(r,t) = -I_b \frac{\Delta}{4\pi r}\left(1 + e^{-t/\tau} \cos\phi\right) . \qquad (20)$$

The time dependence of this term is identical to that of the x or y position signal and will be misinterpreted. For example, suppose that we superimpose this effect with that produced by an offset beam. We find terms like

$$V_m(t) = 2I_b\, e^{-t/\tau}\left(\rho\cos\theta - \frac{\Delta}{4\pi r}\cos(\theta-\phi)\right) \quad . \qquad (21)$$

Here as before the beam is located at the angle θ. Thus the smallest beam offset one can expect to reliably measure is bounded by $\Delta/4\pi$. Therefore, it is important to minimize the foil overlap and to avoid locating it near the pickoff points.

On the ATA and ETA II accelerators, these beam bugs were integrated into computerized data collection systems capable of displaying the beam current and position along the length of these systems. For further descriptions and examples of collected data see reference (8).

BEAM SIZE AND POSITION MEASUREMENTS

Although the beam bugs are useful for finding the centroid of the beam in the accelerator or transport system, they give no information about the size or current density profile of the beam. A common and very useful diagnostic (20) for determining these parameters was to observe the light emitted with a gated TV system as the beam struck the dump or passed through a metal or carbon foil. This diagnostic was in common use after approximately 1970 on all the Livermore electron accelerators. A digital frame grabber/scanning system was use to generate beam profiles or contour plots of the beam current density. For a long time, the physics behind the light emission was not understood. In 1983, not coincidentally during the time R. Fiorito of the Naval Surface Weapons Laboratory was visiting LLNL, the group began to realize that the source of the light was transition radiation emitted as the relativistic beam struck the material. Since then Fiorito and his colleagues have intensively investigated the physics of transition radiation generated by relativistic beams striking foils. The 1993 Faraday Cup prize was awarded to R. Fiorito and D. Rule for the development of diagnostics (21) based on transition radiation.

Another technique developed by Beam Research personnel for determining the profile and position of the electron beam depends on the x-rays generated as a wire is scanned through the beam. The x-rays from the wire are detected by a fast scintillator and photo-multiplier tube. The detector is collimated by lead shielding to minimize X-ray noise from other sources. At the higher ATA beam energies as much a 0.3 m of lead was required to reduce the X-ray noise to acceptable levels. This diagnostic requires many highly repeatable beam pulses as the wire is scanned across the beam. Because of the excellent time response of the X-ray detector, spatial beam profiles can be obtained at any time during the pulse. X-rays are generated by all the electrons that strike along the wire. To obtain true profiles, the data must be unfolded (Abel inversion) This was seldom performed in the actual experiments. A refinement was to use a tungsten or tantalum dot as the X-ray scatterer. The dot was much smaller than the beam and consisted of a small carbon container filled with tungsten or tantalum powder that was suspended by carbon

fibers . The profiles obtained by scanning the dot through the beam require no unfolding but the signal to noise ratio tended to be smaller.

ENERGY MEASUREMENTS

Energy analyzers for induction linacs are similar to those developed for other types of accelerators. I will describe two analyzers developed at LLNL, the first was used with the Astron accelerator with some service on the ETA accelerator. The second was developed for use at energies near 50 MeV on the ATA accelerator.

The Astron on-line beam energy analyzer

This energy analyzer (22) was a spectrometer and as such is similar to several developed by others (23). The analyzer was used in three separate modes. The absolute energy of the beam was determined to within 2%. Relative beam energy variations smaller than 0.1% occurring in times less than 10 nsec could be measured. And the analyzer was used to measure the beam current averaged over a pulse as a function of energy.

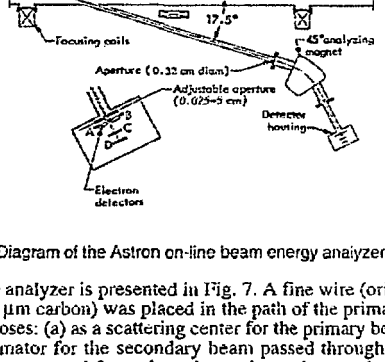

Fig. 7 Diagram of the Astron on-line beam energy analyzer

A diagram of the analyzer is presented in Fig. 7. A fine wire (originally 38 μm tungsten but later 50 μm carbon) was placed in the path of the primary beam. The wire serves two purposes: (a) as a scattering center for the primary beam; and (b) as one part of the collimator for the secondary beam passed through the analyzing magnet. The current scattered from the primary beam is completely negligible (≈0.1%), and thus the analyzer causes no interference with the accelerator operation.

The secondary beam originating at the scattering wire is collimated by a 0.32 cm diameter hole just before the analyzing magnet. Thus the collimating system consists of the tungsten scattering wire and the 0.32 cm bore. The secondary beam is bent 45° and focused by the analyzing magnet. The magnetic field of the

analyzing magnet is measured to 0.01% by a rotating coil Gauss meter. At the detector slit, the magnetic field focuses the beam to a vertical line. That is, a horizontal focus exists at the plane of the A and B detectors.

Detectors A, B, C, and D are 1x0.5x0.05 cm chips of doped silicon which provide approximately 10^5 secondary electrons for each energetic electron striking their surfaces.

An absolute calibration of the system was obtained by allowing X-rays produced by the primary beam to generate neutrons in a block of beryllium. The threshold energy of 1.66 MeV for neutron emission was detected and used to calibrate the analyzer. The calibration thus obtained is believed accurate to 2%.

To determine the absolute energy of the beam to within 2%, the outputs of detectors A and B are electronically subtracted and displayed on an oscilloscope. The signal from detector C is also displayed on the oscilloscope. The absolute energy measurement is obtained by maximizing the signal from detector C and then measuring the magnetic field of the analyzing magnet. The waveform displayed by the A-B signal is then a crude display of the beam energy as a function of time. An example of these signals is given in Fig. 8.

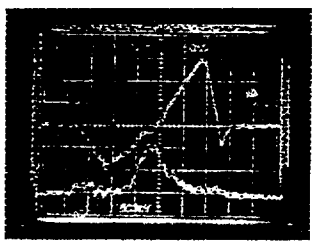

Fig. 8 Analysis of an Astron beam with a large energy spread. Top trace--A-B signal at 0.5 %/div.; bottom trace is C signal; sweep speed 50 ns/div. Beam energy is 5.13 MeV

Measurements of relative beam energy variations smaller than 0.1% occurring in times less than 10 nsec can be obtained by increasing the gain on the A-B signal and recording the time(s) of the zero crossing(s) of the oscilloscope trace as a function of the magnetic field of the analyzing magnet. The percentage change in the magnetic field of the analyzing magnet is then plotted as a function of the recorded zero crossing times resulting in a curve such as that shown in Fig. 9.

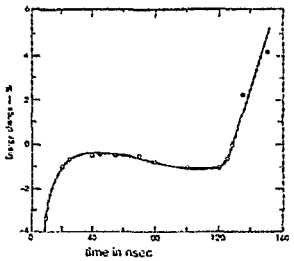

Fig. 9 Change in the Astron beam energy as a function of time.

For more powerful beams at higher beam energies the scattering wire will not survive, and the range of the beam electrons in material becomes impractically long. Sharp beam images can not be produced by aperturing the beam with slits or pinholes because the electrons scatter back into the aperture. As a consequence, standard pepper-pot emittance diagnostic techniques cannot be used and other methods must be found to diagnose the beam. Moreover, at high beam powers the design of a beam dump that will survive the beam becomes as issue. A multi-purpose device was developed for diagnosing the 50 MeV, 10 KAmp ATA beam.

The ATA diagnostic box

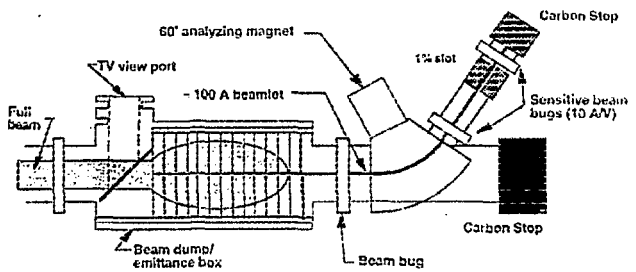

Fig. 10. Sketch of the high power beam dump and diagnostic assembly developed for ATA.

The beam dump/diagnostic system (24) developed for the ATA accelerator consisted of a series of carbon plates whose collective thickness totaled approximately 1.5 ranges at 50 MeV. The dump was designed to dissipate up to 175 kW of average power. The beam power absorbed by the plates was radiated to a water cooled wall. A small hole along the axis of the plates formed a collimator that permitted a low current beamlet to pass through an energy analyzer. The analyzer consists of a 60° bending magnet and two high sensitivity (high resistance) beam bugs. Fig. 10 is a schematic of the assembly.

The beam current and position at the entrance to the dump/diagnostic assembly are measured with a beam bug of the type described above. After passing through the beam bug, the beam enters the dump which consists of a series of range-thin carbon disks. The first disk was placed at an angle of 45° to the beam and used to develop an image of the beam for a gated TV system. A small hole of diameter D (1/4") along the axis through all of the carbon disks is used to form a collimator that produces a beamlet of current determined by the beam emittance ε and the acceptance α of the collimator according to $i = I_b(\alpha/\varepsilon)^2$. The collimator acceptance $\alpha = D^2/4L$ where L is the collimator length.

After leaving the dump, an analyzing magnet bends the beamlet through an angle of 60° into a secondary beam line. The beamlet is detected by a pair of high-sensitivity beam bugs. The first is located close to the exit of the analyzing magnet and measures the total current of the beamlet passing through the collimator. The ratio of the beamlet current to the primary current is used to obtain an estimate of the beam emittance of the on-axis component of the primary beam. The beamlet continues through the secondary beam line and then through a slot designed to accept an energy variation of up to 1%. The second sensitive current monitor is used to measure the time variation of the beamlet within the 1% energy acceptance set by the slot. The beamlet is finally stopped by a six-inch thick (~1.25 ranges) solid carbon dump. X-ray induced noise in the signal cables was a problem near this diagnostic. The X-ray noise was greatly alleviated (25) by adding two inverted negative bug pickoffs to two positive bug pickoffs away from the radiation field.

MAGNETIC FIELD MEASUREMENTS

The measurement of fast magnetic fields is often of interest. Often these are less than ideal, particularly at high frequencies, because the magnetic pickups are also sensitive to electric fields that may also be present. There are at least two possible ways of avoiding the electrical field pickup.

a) Birx loops

D. Birx solved the problem (26) with the design shown in Fig.11. The pickup is shielded from electric fields by equal lengths of metal on each side of the loop. The magnetic field is admitted to the loop interior by the small gap leading to the precisely known area. It is important to locate the gap so that the shield lengths on each side are exactly equal, and the electric field pickup of one side is exactly canceled by pickup from the other. Obtaining the required mechanical precision is a relatively easy task for a machinist.

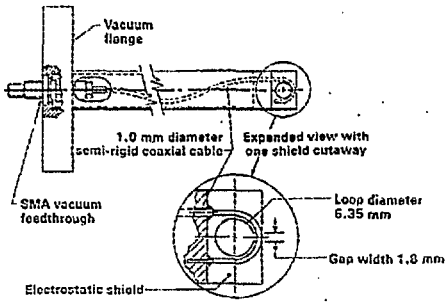

Fig 11 Drawing of a shielded rf pickup loop

b)Shield Integrated Probes

Shield integrated loops (27) were developed for moderately fast magnetic field measurements in particularly harsh environments (i.e. in the presence of strong electric fields and/or energetic electrons). The spurious electric field can be eliminated by placing the magnetic pickup coil within an electrostatic shield. The shield impedes the penetration of the external magnetic field in such a way that for certain periods the field inside the shield is proportional to the integral of the field outside. Since the coil effectively differentiates the field, the detected signal is approximately proportional to the external magnetic field.

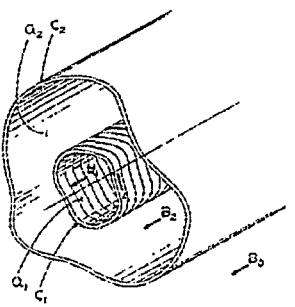

Fig 12 Generic shield-integrated magnetic probe. B_0 is the externally applied field, B_1 is the field within the coil of area a_1, B_2 is the field in the area a_2 between the pickup coil and the shield.

For simplicity consider the case of a long cylindrical coil of N turns and length ℓ enclosed by a good, but not perfect, conducting thin cylindrical shell as shown in Fig. 12. At t=0 an external uniform magnetic field B_0 is applied to the outside of the coil.

The time constant for field penetration of the shield is

$$\tau_s = L_s / R_s = \frac{\sigma \delta \mu_o}{C_2}\left(a_1 + a_2\right) \ . \tag{22}$$

where C2 is the circumference of the shield, δ is the thickness, and σ is the conductivity of the shield material. Similarly, the coil has a time constant determined by its inductance and the resistance in the circuit of

$$\tau_c = L / R = \frac{\mu_o N^2 a_1}{R\ell} \tag{23}$$

Here L is the self-inductance of the coil, ℓ is the length of the shield, and R is the total of the coil resistance R_C plus the resistance R_{EXT} of the external circuit (generally 50 Ω).

Defining α as the ratio of the area inside the coil to the total area ($\alpha = a_1/(a_1 + a_2)$) one can obtain equations for the change in field across the shield and coil

$$B_0 - B_2 = \tau_s \left[(1-\alpha) \frac{\partial B_2}{\partial t} + \alpha \frac{\partial B_1}{\partial t} \right] \tag{24}$$

$$B_2 - B_1 = \tau_c \frac{\partial B_1}{\partial t} \tag{25}$$

These Equations are easily solved for the output voltage in terms of the externally applied field B_0 by Laplace transformation. One obtains for the signal voltage V_0.

$$V_o = -\frac{R_{ext}}{R} \frac{sNa_1 B_o(s)}{\tau_1 \tau_2 \left(s + 1/\tau_1\right)\left(s + 1/\tau_2\right)} \tag{26}$$

In this equation τ_1 and τ_2 are the two solutions of the equation

$$\left(\tau_{1,2}\right)^2 - \tau_{1,2}\left(\tau_c + \tau_s\right) + \tau_c \tau_{s(1-\alpha)} = 0 \tag{27}$$

If, as is generally true, time constants τ_1 and τ_2 are not of comparable magnitude, one finds in terms of the smaller and larger of the time constants τ_s, τ_c.

$$\tau_1 \cong (1-\alpha)\frac{\tau_s\tau_c}{\tau_s+\tau_c} \cong (1-\alpha)\,\tau_{smaller} \tag{28}$$

$$\tau_2 \cong \tau_{larger} \quad . \tag{29}$$

Let us suppose that the external field B_O is switched on at $t = 0$. In this case $B_O(s) = B_O/s$. By Laplace inverting Eq. (13) one obtains

$$V_o(t) \cong -\frac{R_{ext}}{R}\frac{N_s B_o}{\tau_2}\left(e^{-t/\tau_1} - e^{-t/\tau_2}\right) \quad . \tag{30}$$

The rise time of the signal is approximately the smaller of the shield and coil time constants reduced by the factor (1 - α). The fall time is approximately the longer time constant. Note that as the space between the coil and the shield becomes small (α→ 1), the rise time improves.

Notice that there is complete duality between the roles of the shield and coil time constants. The shield and coil time constants affect the system response in an entirely symmetrical way. Depending on relative magnitudes, either could establish the rise time and/or fall time of the probe. This means that there are two methods the experimenter can use to make a self integrating probe. The shield time constant can be made much longer than the L/R time constant of the coil producing a shield-integrated probe. Conversely, as is more commonly done, one can make the coil L/R time constant much longer than the shield time constant producing a coil-integrated probe.

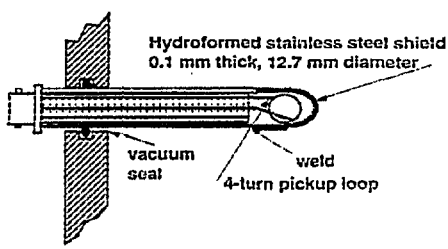

Fig 13 A shield integrated magnetic field probe

The design of a shield-integrated magnetic probe is shown in Fig. 13. This probe was used for measuring the fields created around a 20 ns, 20 kiloamp electron beam. The sensitivity of the probe was 14 Gauss/Volt. The rise time was 7 ns and the fall time set by the shield was near 433 ns. This was extended to approximately 10 μs with a compensating circuit of the type shown in Fig.6a with a corresponding loss of sensitivity.

ACKNOWLEDGMENT

This paper summarizes many contributions made by the experimental physicists that worked in the Astron and Beam Research Programs at the Lawrence Livermore Laboratory from the period 1970 to 1985. It is a pleasure for me to acknowledge the many interactions and exchange of ideas with my colleagues and the particularly significant contributions of B. Stallard, E. Lauer, L. Reginato, J. Clark, D. Birx, K. Struve, Y.P. Chong, and F. Chambers to the diagnostic systems developed at LLNL.

REFERENCES

(1) K Struve, "Electrical Measurement Techniques for Pulsed High Current Electron Beams", submitted to the Measurement of Electrical Quantities in Pulse Power Systems-II, National Bureau of Standards, Gaithersburg, Maryland (1986), also UCRL-93261, LLNL, (1986).

(2) N. C. Christofolis, Proc. U.N. Conf. on Peaceful Uses of Atomic Energy 2nd Geneva, Vol. 32, p 279, (1958).

(3) N. C. Christofolis, R.E. Hester, W.A.S. Lamb, D.D. Reagan, W.A. Sherwood, and R.E. Wright, Rev. Sci. Instrum. 35, 886, (1964).

(4) J.E. Leiss, N.J. Norris, and M.A. Wilson, Part. Accel., 10, 223, (1980).

(5) R. Avery et. al., "The ERA 4 MeV Injector," Proc. of the 1971 PAC, Chicago, IL. (1971) also UCRL-20174, LBL (1971).

(6) R.E. Hester, et al., IEEE Trans. Nucl. Sci. NS-26, 4180, (1979); T.J. Fessenden, et al., IEEE Trans. Nucl. Sci., NS-28, (1981).

(7) B. Kulke, T.G. Innes, R. Kihara, and R.D. Scarpetti, "Initial Performance Parameters on FXR/" Proc. 5th IEEE Power Modulator Symposium, 307, (1982).

(8) L. Reginato, IEEE Trans. Nucl. Sci., NS-30, 2970, (1983).

(9) F.W. Chambers et. al., "Diagnostics and Data Analysis for the ETA II Linear Induction Accelerator," Proc. of the 1991 PAC, San Fransisco, CA., 3085, (1971) and subsequent papers.

(10) R.T. Avery et. al., IEEE Trans. Nucl. Sci., NS-32, 3187, (1985).

(11) A. Friedman et. al., "Recirculating Induction Accelerators for Inertial Fusion: Prospects and Status," Proceedings of the International Symposium on Heavy Ion Inertial Fusion, to be published by Fusion Engineering and Design, (1996).

(12) S. Eylon, "The Diagnostics System for MBE-4," Conference Proceedings No. 252: Beam Instrumentation Workshop, p. 225, AIP (1992).

(13) D. Berners and L. Reginato, "Beam Position and Total Current Monitor for Heavy Ion Fusion Beams," Conference Proceedings No. 281: Beam Instrumentation Workshop, p. 168, AIP (1992).BIW

14) R.T. Avery, A. Faltens, and E.C. Hartwig, "Non-Intercepting Monitor of Beam Current and Position," UCRL-20166, LBL, (1971).

(15) T.J. Fessenden, B. W. Stallard, and G.G. Berg, "Beam Current and Position Monitor for the Astron Accelerator," Rev. of Sci. Instru., 43, 1789, (1972).

(16) K. Struve , "The ATA Beam Bug," informal communication, LLNL.

(17) R.C.Weber, "Longitudinal Emittance---," Conference Proceedings No. 212: Beam Instrumentation Workshop, p. 85, AIP (1989) see page 110.

(18) R. K. Cooper and V.K. Neil, "Resistor Beam bugs," UCID-16057, LLNL, (1972)

(19) T.J. Fessenden, "Beam Bugs--Asymptotic Response," informal communication, LLNL.

(20) Y.P. Chong, R. Kalibjian, J.P.Cornish, J.S. Kallman, and D. Donnelly, "Beam Profile Measurements on the Advanced Test Accelerator using Optical Techniques," p. 738, Proc. of the "Beams 86" Conference, Kobe, Japan, (1986).

(21) R.B. Fiorito and D. W. Rule, "Optical Transition Radiation Beam Emittance Diagnostics," Conference Proceedings No. 319: Beam Instrumentation Workshop, p. 21, AIP (1994) and references therein.

(22) T.J. Fessenden, "The Astron On-Line Beam Energy Analyzer,"Rev. of Sci. Instru., 43, 1090, (1972)

(23) see for instance Ref. (17) p. 96..

(24) J.M. White et. al., "Beam Dump/Diagnostic Box for a 10 kA, 50 MeV, 50 ns Electron Beam," IEEE Trans. Nucl. Sci., NS-30, 2207, (1983).

(25) K. Struve, "Radiation Induced Noise Signals in Diagnostic cabling of the Advanced Test Accelerator," p. 742, Proc. of the "Beams 86" Conference, Kobe, Japan, (1986).

(26) D. Birx private communication

(27) T.J. Fessenden and B.W. Stallard, "Shielded Magnetic Probes for Pulsed Magnetic Field Measurements," UCID- 16115 LLNL, (1972).

3.1 Introduction

It has recently been demonstrated that flavor and CP violations provide an important new probe of supersymmetric grand unified theories [6, 7, 8, 9]. These new signals, such as $\mu \to e\gamma$ and the electron electric dipole moment d_e, are complementary to the classic tests of proton decay, neutrino masses and quark and charged lepton mass relations. The classic tests are very dependent on the flavor interactions and symmetry breaking sector of the unified model: it is only too easy to construct models in which these signals are absent or unobservable. However, they are insensitive to the hardness scale, Λ_H, of supersymmetry breaking.[1] On the other hand, the new flavor and CP violating signals are relatively insensitive to the form of the flavor interactions and unified gauge symmetry breaking, but are absent if the hardness scale, Λ_H, falls beneath the unified scale, M_G. The signals are generated by the unified flavor interactions leaving an imprint on the form of the soft supersymmetry breaking operators [25], which is only possible if supersymmetry breaking is present in the unified theory at scales above M_G.

The flavor and CP violating signals have been computed in the minimal $SU(5)$ and $SO(10)$ models for leptonic [6, 7, 8] and hadronic processes [9], for moderate values of $\tan\beta$, the ratio of the two Higgs vacuum expectation values. While rare muon decays provide an important probe of $SU(5)$, it is the $SO(10)$ theory which is most powerfully tested. If the hardness scale for supersymmetry breaking is large

[1] This is the highest scale at which supersymmetry breaking squark and gluino masses appear in the theory as local interactions